AN ε-UNIFORM FINITE ELEMENT METHOD FOR SINGULARLY PERTURBED TWO-POINT BOUNDARY VALUE PROBLEMS

Q. S. SONG, G. YIN, AND Z. ZHANG

Abstract. This work develops an ε-uniform finite element method for singularly perturbed two-point boundary value problems. A surprising and remarkable observation is illustrated: By inserting one node arbitrarily in any element, the new finite element solution always intersects with the original one at fixed points, and the errors at those points converge at the same rate as regular boundary value problems (without boundary layers). Using this fact, an effective ε-uniform approximation out of boundary layer is proposed by adding one point only in the element that contains the boundary layer. The thickness of the boundary layer need not be known *a priori*. Numerical results are carried out and compared to the Shishkin mesh for demonstration purpose.

Key Words. finite element method, singular perturbation, ε-uniform approximation, layer-adapted mesh, Shishkin mesh.

1. Introduction

This paper is concerned with linear Galerkin finite element method for singularly perturbed boundary value problems (BVPs). Consider a one-dimensional BVP problem

$$(1.1) \qquad -\varepsilon u'' - bu' + cu = f, \quad x \in (0,1); \quad u(0) = u(1) = 0.$$

For simplicity, let $b \leq 0$, $c \geq 0$, and $0 < \varepsilon \ll 1$ be constants such that not both b and c are 0. If $b > 0$, by using substitution $w(x) = u(1-x)$, it reduces to the case with $b \leq 0$. All results presented in this paper can be readily generalized to smooth and non-vanishing functions $b(x)$ and $c(x)$.

If the exact solution $u(\cdot)$ of (1.1) is "bad" in the sense that $\|u''\|_\infty$ is not bounded uniformly in ε, the standard h-version finite element method (FEM) generates huge errors through the whole domain when ε is very small. Typically, it is caused by a small interval of width $O(\varepsilon)$ or $O(\sqrt{\varepsilon})$ (called boundary layer), in which u'' rapidly changes.

To overcome this difficulty for the h-version finite element method, there are roughly two types of methods in the literature: 1) stabilize the approximation by modifying the variational form under quasi-uniform mesh (if we are only interested in the overall behavior of the solution); 2) use anisotropic meshes by putting more grid points in the boundary layer region (if we want to resolve the solution inside

the boundary layer region as well). Many such schemes are extensively studied in the context of singularly perturbed problems since the 1970s; see [1], [3]–[20], and references therein. Among those, upwinding schemes and streamline diffusion finite element methods (SDFEM) are in the first group, while Bakhalov mesh [1] and Shishkin mesh [19] belong to the second group.

Given a partition (or grid)

$$(1.2) \qquad \mathbb{T}^n = \{x_i |\, 0 = x_0 < x_1 < \cdots < x_{n+1} = 1\},$$

we denote the FEM solution of (1.1) on $\mathbb{T}^n$ by u^n, and the interpolation of the exact solution on $\mathbb{T}^n$ by u_I^n. If there is only one boundary layer, both Bakhalov mesh and Shishkin mesh have $n + n$ grid points, with n uniform grids outside the boundary layer region and n grids inside boundary layer region. The n grids inside the boundary layer region are uniform for Shishkin mesh and properly graded for Bakhalov mesh. The *a priori* error estimates are

$$(1.3) \qquad \|u - u^n\|_\infty \le C n^{-2}$$

under Bakhalov mesh, and

$$(1.4) \qquad \|u - u^n\|_\infty \le C n^{-2} \ln^2 n$$

under Shishkin mesh. Here $C > 0$ is independent of ε, and the convergence rates are ε-uniform.

In this article, we propose and analyze a recovery method under uniform or quasi-uniform mesh. This recovery yields ε-uniform convergence in all elements, except the one containing the boundary layer. The convergence rate is the same as using Bakhalov mesh. In addition, we are able to locate a point in each element where the approximation is extremely accurate. The analysis in this article is elementary and the scheme is surprisingly simple. Here is our first algorithm.

Algorithm 1.
- Step 1. Solve the problem by the standard finite element method with n uniform grids. This step is likely to produce an oscillatory solution.
- Step 2. Add an extra grid point anywhere in the element containing the boundary layer, and solve the same problem again. This step produces another solution.
- Step 3. Find intersections of the two solutions in Step 1 and Step 2 in all elements and link those intersections by straight lines.

The above algorithm will produce a highly accurate solution in all but one element. The theoretical foundation will be discussed in Section 3. The key observation is that adding one grid point alters the direction of the oscillation. Therefore, the two solutions always have an intersection in each element except the one containing the boundary layer.

An astonishing discovery is that the intersection point in each element is invariant, i.e., it is independent of the location of the extra grid point in the boundary layer element (the element that contains an boundary layer) and independent of the number of grid points added to the boundary layer element. In other words, no matter how many grid points we add to the boundary layer element and no matter where we put them, those intersections outside the boundary layer element are always the same.

Now let us explain precisely the above description. Without loss of generality, we assume the boundary layer is at $x = 1$. Starting from $\mathbb{T}^n$, we add m points $s_1, \ldots, s_m$ arbitrarily in $(x_n, 1)$ and denote the new partition as $\mathbb{T}^{n+m}$. Then FEM

solutions associated with $\mathbb{T}^n$ and $\mathbb{T}^{n+m}$ intersect at a fixed point $(x(Q_j), y(Q_j))$ in (x_{j-1}, x_j), $j = 2, \ldots, n$. Note that the intersection in the first element is at $x_0 = 0$.

Proposition 1.1. The location of $(x(Q_j), y(Q_j))$ is independent of m and the distribution of $s_1, \ldots, s_m$.

Figure 1-a and Figure 3-a in Section 5 illustrate this fact. Consequently, the following hold.

   a) The accuracy at those intersections are as good as FEM solutions on the grid $\mathbb{T}^{n+m}$ with $m \to \infty$, denoted by $\mathbb{T}^{n+\infty}$, provided the boundary layer is covered by $(x_n, 1)$.
   b) All FEM solutions on $\mathbb{T}^{n+m}$, including solutions with Shishkin mesh and Bakhalov mesh, intersect at the same point in each element (x_{j-1}, x_j), $j = 2, \ldots, n$.

The above properties provide a basis for our recovery method. Among all different FEM solutions, the cheapest one is the solution with $\mathbb{T}^{n+1}$ partition. The recovered approximation value at x_j can be obtained by linear interpolation:

$$(1.5) \qquad \tilde{u}_h(x_j) = y(Q_j) + \frac{y(Q_{j+1}) - y(Q_j)}{x(Q_{j+1}) - x(Q_j)}(x_j - x(Q_j)), \quad j = 2, \ldots, n-1.$$

Since the FEM solution associated with Bakhalov mesh passes $(x(Q_j), y(Q_j))$, we have

$$\|u(x(Q_j)) - y(Q_j)\|_\infty \le Cn^{-2}, \quad j = 1, 2, \ldots, n,$$

due to (1.3).

Our recovery method does not need any stabilization procedure nor does any anisotropic mesh. Even two oscillatory solutions can produce a good recovery. However, we may place the extra grid point in $(x_n, 1)$ cleverly to achieve a better effect.

It has been known for some time that a finite element scheme can be stabilized by having two grid points sufficiently close. In context of the p-version FEM, using only one element at the boundary layer with measure $O(p\sqrt{\varepsilon})$ [16], a robust exponential rate was established for the reaction-diffusion case ($b = 0$, $c \ne 0$) a decade ago. As for the h-version, a theoretical explanation of two grids distance $O(\varepsilon)$ stabilizing the FEM for the convection-diffusion equation can be found in [4].

In lieu of interpolating these intersections, we present a better way to obtain an ε-uniform approximation. By adding one specific point $\hat{s}_1 \in (x_n, 1)$ with $\hat{s}_1 - x_n = O(\varepsilon)$ when $b \ne 0$ or $\hat{s}_1 - x_n = O(\sqrt{\varepsilon})$ when $b = 0$, the interval $(x_n, \hat{s}_1)$ completely blocks the error impact from boundary layer. Furthermore, $\hat{s}_1$ can be obtained precisely by coefficients ε, b, and c. The theoretical result shows that the FEM solution with grid $\mathbb{T}^n \cup \{\hat{s}_1\}$ in $(0, x_n)$ is the same as the FEM solution of

$$(1.6) \qquad -\varepsilon w'' - bw' + cw = f, \quad x \in (0, \hat{s}_1), \quad w(0) = 0, \quad w(\hat{s}_1) = u(\hat{s}_1),$$

where $u(\cdot)$ is the exact solution of (1.1), and thus $w''(\cdot)$ is uniformly bounded. This enables us to use all kinds of standard FEM error analysis in $(0, \hat{s}_1)$, no matter how huge the errors are generated in $(\hat{s}_1, 1)$; see Remark 4.4. In doing so, we do not need to know the thickness of the boundary layer, since $\hat{s}_1$ is not necessarily in the boundary layer.

Based on the above observation, here comes our second algorithm. This procedure will produce an ε-uniform convergence approximation on $(0, x_n)$. The theoretical explanation will be provided in Section 4.

Algorithm 2.

Under the uniform partition $\mathbb{T}_h$, add a special grid point $\hat{s}_1$ (as obtained from Lemma 4.1) in the element containing the boundary layer, then solve the problem.

2. Formulation

Let $H^1 = \{v : v' \in L^2\}$ and $H_0^1 = \{v : v \in H^1, v(0) = v(1) = 0\}$. The weak solution of (1.1) is a function $u \in H_0^1$ satisfying

$$(2.1) \qquad a(u, v) = \varepsilon(u', v') + b(u, v') + c(u, v) = (f, v), \quad \forall v \in H_0^1,$$

where $(\cdot, \cdot)$ is the L^2 inner product.

For a positive integer $n \geq 2$, let $\mathbb{T}^n$ be the partition defined by (1.2) and let $h_i = x_i - x_{i-1}$. By $\phi_i(x)$, we denote the nodal basis function at x_i for $1 \leq i \leq n$. The finite element space is defined by $V^n = \text{Span}\{\phi_1, \phi_2, \ldots, \phi_n\}$. The finite element discretization of (2.1) is to find $u^n = \sum_{i=1}^{n} u_i^n \phi_i \in V^n$ such that

$$(2.2) \qquad \sum_{i=1}^{n} u_i^n a(\phi_i, \phi_j) = (f, \phi_j), \quad j = 1, 2, \ldots, n.$$

Let A be an $n \times n$ matrix having entries $a_{ij} = a(\phi_j, \phi_i)$ with

$$(2.3) \qquad \begin{aligned} a_{ii} &= \varepsilon\left(\frac{1}{h_i} + \frac{1}{h_{i+1}}\right) + \frac{c}{3}(h_i + h_{i+1}), \\ a_{i,i-1} &= -\frac{\varepsilon}{h_i} + \frac{b}{2} + \frac{c}{6}h_i, \\ a_{i,i+1} &= -\frac{\varepsilon}{h_{i+1}} - \frac{b}{2} + \frac{c}{6}h_i, \\ a_{ij} &= 0, \quad \text{if } |i - j| \geq 2; \end{aligned}$$

and let $U^n = (u_1^n, \ldots, u_n^n)'$ and $F = ((f, \phi_1), \ldots, (f, \phi_n))'$ be column vectors. Then, (2.2) is equivalent to the linear system of equations

$$(2.4) \qquad AU^n = F.$$

Throughout this paper, unless otherwise explicitly mentioned, we assume the solution u of (1.1) has a boundary layer at $x = 1$ and x_n is located outside the boundary layer. This is a reasonable assumption due to the very short interval of boundary layer depending on $0 < \varepsilon \ll 1$. All the results below can be obtained analogously for any other layer located in $[0, 1]$.

Let $\mathbb{T}^{n+m} = \mathbb{T}^n \cup \{s_1, \ldots, s_m\}$, where $x_n < s_1 < \cdots < s_m < x_{n+1}$. Denote the nodal basis functions on $\mathbb{T}^{n+m}$ by $\{\phi_1, \ldots, \phi_{n-1}, \tilde{\phi}_n, \phi_{s_1}, \ldots, \phi_{s_m}\}$, where $\tilde{\phi}_n$ and ϕ_{s_i} are nodal basis for x_n and s_i, respectively. Note that the first $n - 1$ nodal basis functions of $\mathbb{T}^{n+m}$ are the same as those of $\mathbb{T}^n$. Let V^{n+m} be the function space with basis $\{\phi_1, \ldots, \phi_{n-1}, \tilde{\phi}_n, \phi_{s_1}, \ldots, \phi_{s_m}\}$. It is obvious that $V^n \subset V^{n+m}$. Write u^{n+m}, the FEM solution of (1.1) in V^{n+m}, as

$$(2.5) \qquad u^{n+m} = \sum_{i=1}^{n-1} u_i^{n+m}\phi_i + u_n^{n+m}\tilde{\phi}_n + \sum_{i=1}^{m} u_{s_i}^{n+m}\phi_{s_i}.$$

In the next section, we fix $\mathbb{T}^n$, and start with observation on the intersections of u^n and u^{n+m} for different $\mathbb{T}^{n+m}$. For convenience, we use $Q_i \in u^n \cap u^{n+m}$ to denote the intersection of u^n and u^{n+m} in the interval (x_{i-1}, x_i), we denote by $x(Q_i)$ and $y(Q_i)$, the x- and y- coordinates of Q_i, respectively. The result shows that the intersections $\{Q_i : 2 \leq i \leq n\}$ are independent of m and distribution of s_i.

Therefore, by adding only one point $\{s_1\}$, we can compute $\{Q_i \in u^n \cap u^{n+1}\}$, and the accuracy of Q_i has the same accuracy as $u^{n+\infty}$.

3. Intersections of u^n and u^{n+m}

Theorem 3.1. Fix $\mathbb{T}^n$. By adding one point $s_1 \in (x_n, 1)$ arbitrarily, we obtain a new partition $\mathbb{T}^{n+1}$. Then the intersection Q_i of u^n and u^{n+1} in the interval (x_{i-1}, x_i) is independent of the choice of s_1 for any $i = 2, 3, \dots, n$. That is, those coordinates of intersections do not depend on the choice of $s_1 \in (x_n, x_{n+1})$.

Proof. Analogous to (2.2), we have a system of linear equations with respect to $\{u_i^{n+1}, i = 1, \dots, n; u_{s_1}^{n+1}\}$ given by
(3.1)
$$\sum_{i=1}^{n-1} u_i^{n+1} a(\phi_i, \phi_j) + u_n^{n+1} a(\tilde{\phi}_n, \phi_j) + u_{s_1}^{n+1} a(\phi_{s_1}, \phi_j) = (f, \phi_j), \quad j = 1, 2, \dots, n-1,$$

(3.2) $$\sum_{i=1}^{n-1} u_i^{n+1} a(\phi_i, \tilde{\phi}_n) + u_n^{n+1} a(\tilde{\phi}_n, \tilde{\phi}_n) + u_{s_1}^{n+1} a(\phi_{s_1}, \tilde{\phi}_n) = (f, \tilde{\phi}_n),$$

and

(3.3) $$\sum_{i=1}^{n-1} u_i^{n+1} a(\phi_i, \phi_{s_1}) + u_n^{n+1} a(\tilde{\phi}_n, \phi_{s_1}) + u_{s_1}^{n+1} a(\phi_{s_1}, \phi_{s_1}) = (f, \phi_{s_1}).$$

Note that for $1 \leq j \leq n-1$, $a(\tilde{\phi}_n, \phi_j) = a(\phi_n, \phi_j)$ and $a(\phi_{s_1}, \phi_j) = 0$, and (3.1) leads to

(3.4) $$\sum_{i=1}^{n} u_i^{n+1} a(\phi_i, \phi_j) = (f, \phi_j), \quad j = 1, 2, \dots, n-1.$$

On the other hand, for $1 \leq i \leq n-1$, $a(\phi_i, \tilde{\phi}_n) = a(\phi_i, \phi_n)$, and (3.2) yields

(3.5) $$\sum_{i=1}^{n-1} u_i^{n+1} a(\phi_i, \phi_n) + u_n^{n+1} a(\tilde{\phi}_n, \tilde{\phi}_n) = (f, \tilde{\phi}_n) - u_{s_1}^{n+1} a(\phi_{s_1}, \tilde{\phi}_n).$$

For $1 \leq i \leq n-1$, $a(\phi_i, \phi_{s_1}) = 0$, so it follows from (3.3),

(3.6) $$u_n^{n+1} a(\tilde{\phi}_n, \phi_{s_1}) = (f, \phi_{s_1}) - u_{s_1}^{n+1} a(\phi_{s_1}, \phi_{s_1}).$$

Let $p = (1 - s_1)/h_{n+1}$. Observe $\phi_n = \tilde{\phi}_n + p\phi_{s_1}$. Combining two equations above according to (3.5)+$p*$(3.6), we have

(3.7) $$\sum_{i=1}^{n-1} u_i^{n+1} a(\phi_i, \phi_n) + u_n^{n+1} a(\tilde{\phi}_n, \phi_n) = (f, \phi_n) - u_{s_1}^{n+1} a(\phi_{s_1}, \phi_n).$$

Hence,

(3.8) $$\sum_{i=1}^{n} u_i^{n+1} a(\phi_i, \phi_n) = (f, \phi_n) - u_{s_1}^{n+1} a(\phi_{s_1}, \phi_n) + p u_n^{n+1} a(\phi_{s_1}, \phi_n).$$

Let $U^{n+1} = (u_1^{n+1}, \dots, u_n^{n+1})'$ be a column vector with length n. By (3.4) and (3.8),

(3.9) $$AU^{n+1} = \tilde{F},$$

where $\tilde{F}$ is a column vector with left-hand side of (3.4) and (3.8) as elements. Subtracting (3.9) from (2.4),

$$(3.10) \qquad A(U^n - U^{n+1}) = F - \tilde{F} = C_{s,1}\boldsymbol{e}_n,$$

where $\boldsymbol{e}_1 = (1, 0, \ldots, 0)$, $\ldots$, $\boldsymbol{e}_n = (0, \ldots, 0, 1)'$ are standard unit vectors, and

$$(3.11) \qquad C_{s,1} = u_{s_1}^{n+1}a(\phi_{s_1}, \phi_n) - pu_n^{n+1}a(\phi_{s_1}, \phi_n)$$

is a scalar depending only on s_1, since u_n^{n+1} in (3.11) can be determined by s_1 from

$$a(\phi_n, \phi_{s_1})u_n^{n+1} + a(\phi_{s_1}, \phi_{s_1})u_{s_1}^{n+1} = (f, \phi_{s_1}).$$

We see from (3.10) that $U^n - U^{n+1} = C_{s,1}g^n$, where $g^n = (g_1^n, g_2^n, \cdots, g_n^n)'$ is the nodal-value vector of the discrete Green's function $g^n \in V^n$ that solves

$$(3.12) \qquad a(g^n, v) = v(x_n) \quad \forall v \in V^n.$$

The difference $u^n(x) - u^{n+1}(x) = 0$ if and only if $g^n(x) = 0$. Since g^n is independent of s_1, so is the intersections of $u^n - u^{n+1}$. $\square$

Remark 3.2. If g_i^n and g_{i+1}^n have opposite signs, then u^n and u^{n+1} have an intersection in (x_i, x_{i+1}). Moreover, if there is no intersection in some interval (x_i, x_{i+1}) for a choice of s_1, then there will be no intersection for any choice of s_1.

The following Lemma guarantees that g_i^n and g_{i+1}^n have opposite signs under the assumption $c = 0$ for uniform grids and $\varepsilon \ll 1$. The case $c \neq 0$ can be established by perturbation argument for sufficiently small h.

First we simplify the problem. Denote

$$s = -\frac{\varepsilon}{h} - \frac{b}{2} = \frac{|b|}{2} - \frac{\varepsilon}{h},$$

and assume that $s > 0$. For a convection dominated problem, $s > 0$ for a large range of h. Therefore, it is not a restriction in practice.

Dividing each term of the matrix A by s, we end up with an $n \times n$ matrix

$$(3.13) \qquad A_n = \begin{pmatrix} t & 1 & & & & \\ -1-t & t & 1 & & & \\ & \ddots & \ddots & \ddots & & \\ & & -1-t & t & 1 \\ & & & -1-t & t \end{pmatrix}.$$

For convenience, we say a vector $Z = (z_1, \ldots, z_n)$ is an *oscillation* vector, if $z_i z_{i+1} < 0$ for all $1 \leq i \leq n - 1$.

Lemma 3.3. Let $n \geq 2$ be an integer, $t \in (0, 1)$, and $Z = (z_1, \ldots, z_n)'$ be the solution of linear system $A_n Z = \boldsymbol{e}_n$. Then Z is an oscillation vector.

Proof. Let $n = 2$, the solution of $A_2 Z = \boldsymbol{e}_2$ is oscillation, with $z_2 > 0$. Next we use mathematical induction. Assume the solution $\tilde{Z}$ of $A_n \tilde{Z} = \boldsymbol{e}_n$ is an oscillation with nth element is positive.

Consider the solution $Z = (z_1, \ldots, z_{n+1})'$ of

$$(3.14) \qquad A_{n+1} Z = \boldsymbol{e}_{n+1}.$$

Denote $(z_1, \ldots, z_n)'$ by $\bar{Z}$. Then $\bar{Z}$ is the solution of $A_n \bar{Z} = -z_{n+1}\boldsymbol{e}_n$. By assumption of step n, $\bar{Z}$ is an oscillation.

(1) If $z_{n+1} = 0$, then $A_n \bar{Z} = 0$, and we know A_n is a full rank matrix. So $\bar{Z} = 0$, that is $Z = 0$. This is a contradiction to (3.14).

(2) If $z_{n+1} < 0$, by assumption for step n, $\bar{Z}$ is oscillation with $z_n > 0$. Hence $A_{n+1} Z$ is a vector with last element $(-1 - t)z_n + tz_{n+1}$, which is strictly less than zero. This is a contradiction to (3.14), since the last element of left-hand side of (3.14) is 1.

(3) The last case is $z_{n+1} > 0$. Then $\bar{Z}$ is oscillation with $z_n < 0$ by assumption for step n. This implies Z, the solution of (3.14), is an oscillation with last element being strictly positive.

This completes the proof. $\square$

Theorem 3.4. Fix $\mathbb{T}^n$. Let $\mathbb{T}^{n+m} = \mathbb{T}^n \cup \{s_1 < s_2 < \cdots < s_m\}$, where $s_i \in (x_n, 1)$. Then the intersection Q_i of u^n and u^{n+m} in the interval (x_{i-1}, x_i) is independent of m and distribution of $\{s_i\}$ for any $i = 2, 3, \ldots, n$.

Proof. Let V^{n+m} be a function space with nodal basis functions

$$\{\phi_1, \ldots, \phi_{n-1}, \tilde{\phi}_n, \phi_{s_1}, \ldots, \phi_{s_m}\}$$

associated wit $\mathbb{T}_{n+m}$. Analogous to (3.4), we have

$$(3.15) \qquad \sum_{i=1}^{n} u_i^{n+m} a(\phi_i, \phi_j) = (f, \phi_j), \quad j = 1, 2, \ldots, n-1.$$

Since $V^{n+m} \supset V^n$, there exists a linear combination

$$\phi_n = \tilde{\phi}_n + \sum_{i=1}^{m} p_i \tilde{\phi}_{s_i}, \quad p_1, p_2, \ldots, p_m \in [0, 1].$$

Applying similar arguments as that of Theorem 3.1, we obtain

$$(3.16) \qquad \sum_{i=1}^{n} u_i^{n+m} a(\phi_i, \phi_n) = (f, \phi_n) + \sum_{i=1}^{m} (p_i u_n^{n+m} - u_{s_i}^{n+m}) a(\phi_{s_i}, \phi_n).$$

Define $C_{s,m} = \sum_{i=1}^{m} (u_{s_i}^{n+m} - p_i u_n^{n+m}) a(\phi_{s_i}, \phi_n)$. We have

$$(3.17) \qquad A(U^n - U^{n+m}) = C_{s,m} \boldsymbol{e}_n.$$

Hence, the result follows. $\square$

Corollary 3.5. Fix $\mathbb{T}^n$. Let $\mathbb{T}^{n+m} = \mathbb{T}^n \cup \{s_1 < s_2 < \cdots < s_m\}$, where $s_i \in (0, x_1)$. Then the intersection Q_i of u^n and u^{n+m} in the interval (x_{i-1}, x_i) is independent of m and distribution of $\{s_i\}$, and is fixed for any $i = 2, \ldots, n$.

Proof. We rearrange the order of the index from $\{0, 1, 2, \ldots, n, n+1\}$ to $\{n+1, n, \ldots, 1, 0\}$, and change the coordinate linearly from $[0, 1]$ into $[1, 0]$. Using the same line of argument as that of Theorem 3.4, the result holds. $\square$

Corollary 3.6. Fix $\mathbb{T}^n$. Let $\mathbb{T}^{n+m} = \mathbb{T}^n \cup \{s_1 < s_2 < \cdots < s_m\}$, where $s_i \in (x_{k-1}, x_k)$ for some $2 \leq k \leq n$. Then the intersection of u^n and u^{n+m} in the interval (x_{i-1}, x_i) is independent of m and distribution of $\{s_i\}$ for any $i \in \{2, \ldots, n\} \setminus \{k\}$.

Proof. This is straight forward by virtue of Theorem 3.4 and Corollary 3.5. $\square$

The following theorem is a direct consequence of using the Bakhalov mesh.

Theorem 3.7. Assume $\mathbb{T}^n$ is a uniform grid in $[0, 1]$, and the boundary layer is at $x = 1$. Then

$$(3.18) \qquad \max_{1 \leq i \leq n-1} |u^n(x(Q_i)) - u_I^n(x(Q_i))| < Cn^{-2},$$

where C is independent of ε, and $u_I^n \in V^n$ in the interpolation of u on $\mathbb{T}^n$.

Proof. We put $m = O(n)$ grid in $(x_n, 1)$, so that $\mathbb{T}^{n+m}$ forms Bakhvalov grid. The uniform convergence of u^{n+m} on $\mathbb{T}^{n+m}$ is well known (see, e.g., [8, 12]) as

$$(3.19) \qquad \|u^{n+m} - u_I^{n+m}\|_\infty \leq Cn^{-2}.$$

Also, we have $Q_i \in u^{n+m} \cap u^n$ by Corollary 3.6. So

$$(3.20) \qquad |u^{n+m}(x(Q_i)) - u_I^{n+m}(x(Q_i))| \leq Cn^{-2}.$$

Note that $u_I^{n+m}|_{(0,x_n)} = u_I^n|_{(0,x_n)}$. On the other hand, $u^n(x(Q_i)) = u^{n+m}(x(Q_i))$ by Theorem 3.4. Thus, the conclusion follows. $\qquad \square$

Remark 3.8. From the result of Theorem 3.7, we have estimation of $O(n^{-2})$. For non-uniform cases, we can obtain an error bound $O(n^{-1})$ directly from [4].

4. An ε-uniform Approximation u^{n+1} in $(0, x_n)$

In the previous section, by arbitrarily choosing a point $s_1 \in (x_n, 1)$, we can determine $Q_i \in u^n \cap u^{n+1}$ in each interval, and the result shows $u^n(x(Q_i))$ has the same accuracy as that of $u^{n+\infty}$. In this section, by choosing appropriate $\hat{s}_1 \in (x_n, 1)$, we obtain $\hat{u}^{n+1}$, which has ε-uniform accuracy not only at some isolated points $x(Q_i)$ but also on the whole interval $[0, x_n]$. For simplicity, we slightly abuse notation by letting $a_{n,\hat{s}_i} = a(\phi_{\hat{s}_i}, \phi_n)$.

Lemma 4.1. There exists $\hat{s}_1 \in (x_n, 1)$ such that $a_{n,\hat{s}_1} = 0$ for $\hat{\mathbb{T}}^{n+1} = \{x_0 < x_1 < \cdots < x_n < \hat{s}_1 < x_{n+1}\}$.

Proof. By (2.3), to establish the desired result, it is equivalent to prove that there exists $0 < h_{\hat{s}_1} < 1 - x_n$ satisfying

$$(4.1) \qquad -\frac{\varepsilon}{h_{\hat{s}_1}} - \frac{b}{2} + \frac{c}{6} h_{\hat{s}_1} = 0,$$

where $h_{\hat{s}_1} = \hat{s}_1 - x_n$. By eliminating the denominators in the equation (4.1), we have

$$(4.2) \qquad ch_{\hat{s}_1}^2 - 3bh_{\hat{s}_1} - 6\varepsilon = 0.$$

Write $h_{\hat{s}_1}$ using quadratic formula,

$$(4.3) \qquad 0 < h_{\hat{s}_1} = \frac{3b + \sqrt{9b^2 + 24\varepsilon c}}{2c} = \frac{12\varepsilon}{3|b| + \sqrt{9b^2 + 24\varepsilon c}}.$$

Thus,

$$h_{\hat{s}_1} \approx \frac{2\varepsilon}{|b|} \quad \text{for} \quad b \neq 0; \qquad h_{\hat{s}_1} = \sqrt{\frac{6\varepsilon}{c}} \quad \text{for} \quad b = 0.$$

The proof is thus concluded. $\qquad \square$

Remark 4.2. The essence of Lemma 4.1 is to find such a $h_{\hat{s}_1}$ with $a_{n,\hat{s}_1} = 0$. If b and c are not constant, we can compute $h_{\hat{s}_1}$ in which integrations are involved. It is also possible to find it by discretizations.

Theorem 4.3. Given $\mathbb{T}^n$, take $\hat{\mathbb{T}}^{n+1}$ and $\hat{s}_1$ as in Lemma 4.1. Use $\hat{u}^{n+1}$ to denote the FEM solution on $\hat{\mathbb{T}}^{n+1}$ of (1.1). Consider another boundary value problem

(4.4) $\qquad -\varepsilon w'' - bw' + cw = f \quad x \in (0, \hat{s}_1), \qquad w(0) = 0, \quad w(\hat{s}_1) = u(\hat{s}_1),$

where $u(\cdot)$ is a solution of (1.1). Using w^n to denote the FEM solution of (4.4) on $\hat{\mathbb{T}}^{n+1} \setminus \{1\}$, then

(4.5) $\qquad\qquad\qquad\qquad w(x) = u(x), \quad \forall x \in [0, \hat{s}_1],$

and

(4.6) $\qquad\qquad\qquad\qquad \hat{u}^{n+1}(x) = w^n(x), \quad \forall x \in [0, x_n].$

Proof. Note that $(\hat{u}_1^{n+1}, \hat{u}_2^{n+1}, \ldots, \hat{u}_n^{n+1})$ is a solution of the system of linear equations

(4.7) $\qquad \begin{cases} a_{i,i-1}\hat{u}_{i-1}^{n+1} + a_{i,i}\hat{u}_i^{n+1} + a_{i,i+1}\hat{u}_{i+1}^{n+1} = (f, \phi_i) \quad i = 1, 2, \ldots, n-1, \\ \tilde{a}_{n,n-1}\hat{u}_{n-1}^{n+1} + \tilde{a}_{n,n}\hat{u}_n^{n+1} = (f, \tilde{\phi}_n) - a_{n,\hat{s}_1}\hat{u}_{\hat{s}_1}^{n+1}, \end{cases}$

where $\tilde{a}_{n,n-1} = a(\phi_{n-1}, \tilde{\phi}_n)$ and $\tilde{a}_{n,n} = a(\tilde{\phi}_n, \tilde{\phi}_n)$. Let $w^n = \sum_{i=1}^{n-1} w_i^n \phi_i + w_n^n \tilde{\phi}_n + w_{\hat{s}_1}^n \phi_{\hat{s}_1}^-$, where $\phi_{\hat{s}_1}^- = \phi_{\hat{s}_1}|_{[0,\hat{s}_1]}$. Then w_i^n for $i \in \{1, 2, \ldots, n, \hat{s}_1\}$ is a solution of the system of linear equations

(4.8) $\qquad \begin{cases} a_{i,i-1}w_{i-1}^n + a_{i,i}w_i^n + a_{i,i+1}w_{i+1}^n = (f, \phi_i) \quad i = 1, 2, \ldots, n-1 \\ \tilde{a}_{n,n-1}w_{n-1}^n + \tilde{a}_{n,n}w_n^n = (f, \tilde{\phi}_n) - a_{n,\hat{s}_1}w_{\hat{s}_1}^n \\ w_{\hat{s}_1}^n = u(\hat{s}_1). \end{cases}$

The solutions of (4.7) and (4.8) are precisely the same, since $a_{n,\hat{s}_1} = 0$. $\qquad\square$

Remark 4.4. From Theorem 4.3, we can separate the boundary layer by adding a special point $\hat{s}_1 \in (x_n, 1)$ and make it equivalent to solving a non-singularly perturbed BVP by the FEM on $(0, x_n)$. Therefore, the standard FEM error analysis applies as if there were no boundary layer. For example, if $\mathbb{T}_h$ is a uniform partition of $(0, x_n)$, then

$$\|u - \hat{u}^{n+1}\|_{\infty, [0,x_n]} \le Cn^{-2} \|u''\|_{\infty, [0, x_n + O(\sqrt{\varepsilon})]},$$

and $\|u''\|_{\infty, [0, x_n + O(\sqrt{\varepsilon})]}$ is ε-uniformly bounded.

5. Numerical Results

In this section, we present two examples. One is a convection-diffusion equation, another is a reaction-diffusion equation.

Example 5.1. Consider the convection-diffusion equation:

(5.1) $\qquad\qquad\qquad\qquad -\varepsilon u'' + u' = x, \quad u(0) = u(1) = 0.$

The exact solution is

(5.2) $\qquad\qquad u = x\left(\frac{x}{2} + \varepsilon\right) - \left(\frac{1}{2} + \varepsilon\right)\left(\frac{e^{(x-1)/\varepsilon} - e^{-1/\varepsilon}}{1 - e^{-1/\varepsilon}}\right).$

The solution $u(\cdot)$ has a boundary layer at $x = 1$, and is nearly quadratic outside the boundary layer.

First, we use the linear finite element method on two different grid $\mathbb{T}^{15}$ and $\mathbb{T}^{15+1}$ for $\varepsilon = 10^{-3}$, where $\mathbb{T}^{15}$ is a uniform mesh on $[0, 1]$ with 16 intervals, and $\mathbb{T}^{15+1}$ is a modified $\mathbb{T}^{15}$ with one point added at the center of the last interval. The intersections of finite element solution u^{15} and u^{15+1} are almost on the interpolation of exact solution u_I^{15+1}, as shown in Figure 1-a.

Second, we use the grid $\hat{\mathbb{T}}^{15+1}$ to compute for the same ε, where $\hat{\mathbb{T}}^{15+1}$ is modified from $\mathbb{T}^{15}$ by adding one specific point $\hat{s_1} \in (x_n, 1)$ with $\hat{s_1} - x_n = 2\varepsilon$, see Lemma 4.1. The finite element solution $\hat{u}^{15+1}$ is almost overlapped with interpolation of the exact solution u_I^{15} in $[0, x_n]$, as seen from Figure 1-b. This verifies Theorem 4.3.
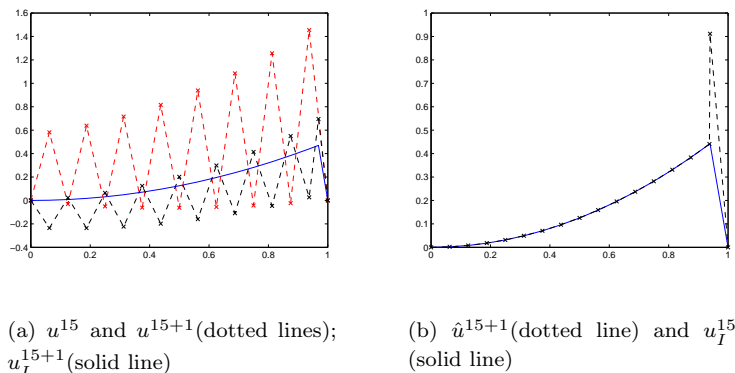

(a) u^{15} and u^{15+1}(dotted lines); u_I^{15+1}(solid line)

(b) $\hat{u}^{15+1}$(dotted line) and u_I^{15} (solid line)

FIGURE 1. FEMs with $\varepsilon = 10^{-3}$ for Example 5.1

To compare with the well-known Shishkin mesh, we construct $\mathbb{T}_s^{n+n}$, which divides both $[0, 1-\theta]$ and $[1-\theta, 1]$ into n equidistant subintervals, where $\theta = \min\{2^{-1}, 2\varepsilon|b|^{-1}\ln(2n)\}$. u_s^{n+n} is used to denote the FEM solution on $\mathbb{T}_s^{n+n}$. Table 1 shows the maximum norm of $u_I^{n+1} - \hat{u}^{n+1}$ and $u_I^{n+1} - u_s^{n+n}$ in $[0, x_n]$. Apparently, both $\hat{u}^{n+1}$ and u_s^{n+n} have ε-uniform accuracy. Moreover, $\hat{u}^{n+1}$ has the same accuracy as that of u_s^{n+n} by using less grids. The reason is that $\hat{u}^{n+1}$ is completely isolated from the impact of errors from boundary layer; see Table 1. This also verifies Theorem 4.3.

n	$\varepsilon = 10^{-5}$		$\varepsilon = 10^{-10}$	
	$\|u_I^{n+1} - \hat{u}^{n+1}\|$	$\|u_I^{n+1} - u_s^{n+n}\|$	$\|u_I^{n+1} - \hat{u}^{n+1}\|$	$\|u_I^{n+1} - u_s^{n+n}\|$
4	6.663e-003	1.117e-002	6.667e-003	1.117e-002
8	2.054e-003	1.567e-003	2.058e-003	1.569e-003
16	5.734e-004	3.480e-004	5.767e-004	3.500e-004
32	1.498e-004	8.384e-005	1.530e-004	8.569e-005
64	3.637e-005	1.948e-005	3.941e-005	2.115e-005
128	7.569e-006	3.928e-006	9.974e-006	5.221e-006
256	1.340e-006	1.340e-006	2.482e-006	1.292e-006
512	3.102e-007	6.738e-007	5.919e-007	3.208e-007

TABLE 1. $\hat{u}^{n+1}$ and u_s^{n+n} are FEM solutions on $\hat{\mathbb{T}}^{n+1}$ and Shishkin mesh $\mathbb{T}_s^{n+n}$ for Example 5.1; $\|\cdot\|$ denote $\|\cdot\|_{\infty,[0,x_n]}$

Let $\varepsilon = 10^{-10}$. Table 2 shows the accuracy of Q_i, the intersections of u^8 and u^{8+1}. Denote x- and y- coordinates of Q_i by $x(Q_i)$ and $y(Q_i)$, respectively.

For $\varepsilon = 10^{-5}$ and $\varepsilon = 10^{-10}$, we compute discrete maximum norm of errors at $\{Q_i\}$ for various n, that is, $\max\limits_{1<i<n} |(u_I^{n+1} - u^{n+1})(Q_i)|$ for various n. At those intersections $\{Q_i\}$, the errors are normally less than 10^{-10}.

i	$x(Q_i)$	$|y(Q_i) - u(x(Q_i))|$	$|y(Q_i) - u_I^8(x(Q_i))|$
2	0.2499999996000000	7.499999579718697e-011	4.999999719812465e-011
3	0.2500000004000000	2.500008533523612e-011	8.326672684688674e-017
4	0.4999999992000000	3.500000012035542e-010	2.999999970665357e-010
5	0.5000000008000000	5.000011515932101e-011	1.110223024625157e-016
6	0.7499999988000000	6.625580639685325e-009	6.700580590379701e-009
7	0.7500000012000000	7.500006171667906e-011	1.110223024625157e-016

TABLE 2. Errors at Q_i with $\varepsilon = 10^{-10}$ on $\mathbb{T}^8$ and $\mathbb{T}^{8+1}$ for Example 5.1.

Plotted in Figure 2-a are the convergence curves (loglog chart) in the maximum norm $\|u_I^{n+1} - \hat{u}^{n+1}\|_{\infty,[0,x_n]}$ for $\varepsilon = 10^{-5}$ and $\varepsilon = 10^{-10}$ based on the errors shown in Table 1, respectively. They clearly indicate the convergence rate is proportional to n^{-2}. It verifies Remark 4.4. Moreover, Figure 2-b are the convergence curves in the discrete maximum norm at $\{Q_i\}$. The curve for $\varepsilon = 10^{-5}$ is not parallel to that of n^{-2}, since the errors of digital computer error is dominant over the algorithm error within 10^{-12}.

Although $\hat{u}^{n+1}$ is uniformly convergent on $(0, x_n)$, $u^{n+1}(x(Q_i))$ is nevertheless much more accurate.

(a) $\|u_I^{n+1} - \hat{u}^{n+1}\|_{\infty,[0,x_n]}$ for various n

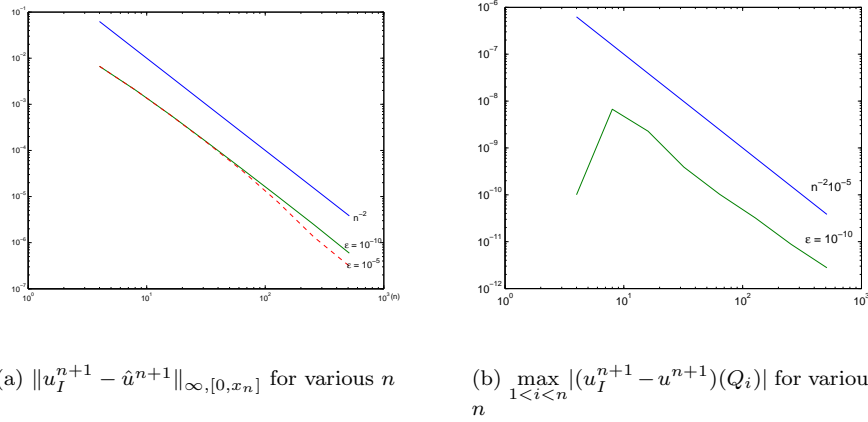(b) $\max\limits_{1<i<n} |(u_I^{n+1} - u^{n+1})(Q_i)|$ for various n

FIGURE 2. Convergence curves with $\varepsilon = 10^{-5}$ and $\varepsilon = 10^{-10}$ for Example 5.1

Example 5.2. We examine the problem of a reaction diffusion equation as another example of (1.1).

(5.3) $-\varepsilon u''(x) + u(x) = x, \quad u(0) = u(1) = 0.$

The exact solution is

(5.4) $u(x) = x - \dfrac{e^{(x-1)/\sqrt{\varepsilon}} - e^{-(x+1)/\sqrt{\varepsilon}}}{1 - e^{-2/\sqrt{\varepsilon}}}.$

The exact solution $u(\cdot)$ has a boundary layer at $x = 1$, and is nearly linear outside the boundary layer. Also, reaction diffusion equation has relatively stable matrix A compared with convection diffusion equation. Due to these reasons, the FEM solutions of (5.3) is more accurate than the FEM solutions of (5.1).

For $\varepsilon = 10^{-10}$, we compute the FEM solution u^4 and u^{4+1} on the grid $\mathbb{T}^4$ and $\mathbb{T}^{4+1}$, where $\mathbb{T}^4$ is a uniform mesh on $[0,1]$ and $\mathbb{T}^{4+1}$ is modified by adding one point at the center of the last interval; see Figure 3-a.

By adding one point $\hat{s}_1 \in (x_n, 1)$ with $\hat{s}_1 - x_n = \sqrt{6\varepsilon}$ as in Lemma 4.1, we use new grid $\hat{\mathbb{T}}^{n+1}$, and denote its FEM solution as $\hat{u}^{4+1}$. As shown in Figure 3-b, $\hat{u}^{4+1}$ is almost overlapped with u_I^4, the interpolation of exact solution; see Figure 3-b.
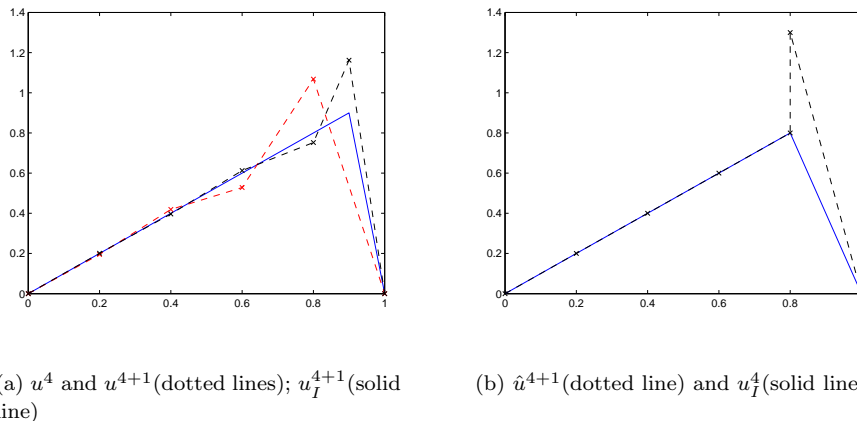

(a) u^4 and u^{4+1}(dotted lines); u_I^{4+1}(solid line)   (b) $\hat{u}^{4+1}$(dotted line) and u_I^4(solid line)

FIGURE 3. FEMs with $\varepsilon = 10^{-10}$ for Example 5.2.

Let $\theta = \min\{\, 2^{-1}, \sqrt{\varepsilon/c}\ln(2n)\}$. We construct shishkin mesh $\mathbb{T}_s^{n+n}$ by dividing $[0, 1-\theta]$ and $[1-\theta, 1]$ into n equidistant subintervals. Table 3 present the errors of $\hat{u}^{n+1}$. Compared with u_s^{n+n}, the errors of the FEM solutions using Shishkin mesh $\mathbb{T}_s^{n+n}$ are smaller and ε-uniform. We omit the convergence curve and error table of Q_i, since all those errors are within computer errors (around 10^{-14}).

6. Concluding Remarks

This paper has been devoted to finite element methods for singularly perturbed boundary value problems. An interesting behavior is discovered: One can add arbitrary many points in one element, while the corresponding FEM solutions always have the common intersections $\{Q_i\}$ in all other elements. Based upon this phenomenon, a practical and efficient ε-uniform mesh is developed. The FEM solution under this mesh can be viewed as a non-singularly perturbed BVP problem, and all general FEM error analysis can be applied.

n	$\varepsilon = 10^{-5}$		$\varepsilon = 10^{-10}$	
	$\|u_I^{n+1} - \hat{u}^{n+1}\|$	$\|u_I^{n+1} - u_s^{n+n}\|$	$\|u_I^{n+1} - \hat{u}^{n+1}\|$	$\|u_I^{n+1} - u_s^{n+n}\|$
4	1.665e-016	1.517e-004	1.110e-016	4.980e-007
8	1.110e-016	5.415e-005	2.220e-016	1.868e-007
16	2.220e-016	2.161e-005	3.331e-016	8.451e-008
32	2.220e-016	7.391e-006	3.331e-016	4.054e-008
64	3.331e-016	1.300e-006	5.551e-016	1.984e-008
128	4.441e-016	1.159e-009	5.551e-016	5.551e-016
256	2.459e-013	2.948e-007	6.661e-016	9.795e-009
512	5.440e-015	2.865e-007	7.772e-016	4.847e-009

TABLE 3. $\hat{u}^{n+1}$ and u_s^{n+n} are the FEM solutions on $\hat{\mathbb{T}}^{n+1}$ and Shishkin mesh $\mathbb{T}_s^{n+n}$ for Example 5.2; $\|\cdot\|$ denotes $\|\cdot\|_{\infty,[0,x_n]}$.

It should be noted that if the exact solution has several layers, our method can be generalized to isolate each layer. Finally, to generalize the idea to isolate boundary layers in higher dimensional problems remains to be a very challenging task.

References

[1] N.S. Bakhalov, Towards optimization of methods for solving boundary value problems in the presence of boundary layers, *Zh. Vychisl. Mater. Mater. Fiz.*, **9** (1969), 841-859, in Russian.

[2] S.C. Brenner and L.R. Scott, *The mathematical Theory of Finite Element Methods*, Springer, 2002.

[3] F. Brezzi, T.J.R. Hughes, L.D. Marini, A. Russo, and E. Süli, A priori error analysis of residual-free bubbles for advection-diffusion problems, *SIAM J. Numer. Anal.*, **39**(4) (1999), 1933-1948.

[4] L. Chen and J. Xu, Stability and accuracy of adapted finite element methods for sigularly perturbed problems, *Numerische Mathematik*, preprint.

[5] E.P. Doolan, J.J.H. Miller, and W.H.A. Schilders, *Uniform numerical methods for problems with initial and boundary layers*, Boole Press, Bublin, (1980).

[6] W. Huang, Variational mesh adaptation: isotropy and equidistribution, *J. Comput. Phys.*, **174** (2001), 903-924.

[7] C. Johnson, A. Schatz, and L. Wahlbin, Crosswind smear and pointwise errors in the streamline diffusion finite element method, *Math. Comp.*, **49** (1987), 25-38.

[8] N.V. Kopteva. Uniform convergence with respect to a small parameter of a scheme with central difference on refining grids, *Comput. Math. Phys.*, **39** (1999), 1594-1610.

[9] N.V. Kopteva. Maximum norm a posteriori error estimates for a one-dimensional convection-diffusion problem, *SIAM J. Numer. Anal.*, **39** (2001), 423-441.

[10] K.W. Morton, *Numerical Solution of Convection-Diffusion Problems*, Chapman and Hall, London, 1996.

[11] T. Linss. Layer-adapted meshes for convection-diffusion problems, *Comput. Methods Appl. Mech. Engrg.*, **192** (2003), 1061-1105.

[12] J.J.H. Miller, E. O'Riordan, and G.I. Shishkin. *Fitted Numerical Methods for Singular Perturbation Problems.* World Scientific, 1996.

[13] E. O'Riordan and M. Stynes, Auniformly accurate finite element method for a singularly perturbed one-dimensional reaction-diffusion problem, *Math. Comp.* **47** (1986), 555-570.

[14] Y. Qiu, D.M. Sloan, and T. Tang, Numerical solution of perturbed two-point boundary value problem using equidistribution: analysis of convergence, *J. Comput. Appl. Math.*, **116** (2000), 121-143.

[15] A.H. Schatz and L.B. Wahlbin, On the finite element method for singularly perturbed reaction-diffusion problems in two and one dimensions, *Math. Comp.*, **40** (1983), 47-89.

[16] C. Schwab and M. Suri, The *p* and *hp* versions of the finite element method for problems with boundary layers, *Math. Comp.*, **65** (1996), 1403-1429.

[17] H.-G. Roos, M. Stynes, and L. Tobiska, *Numerical methods for singularly purturbed differential equations: Convection-diffusion and flow problems* . Springer, 1996.

[18] H.-G. Roos, Layer-adapted grids for singular perturbation problems, *ZA-MMZ Angew Math Mech.*, **78-5** (1998), 291–309.

[19] G.I. Shishkin, *Grid approximation of sigulary perturbed elliptic and parabolic equations*, PhD thesis, Second doctorial thesis, Keldysh Institute, Moscow, 1990, in Russian.

[20] Z. Zhang, Finite elment superconvergence approximation for one-dimensional singularly perturbed problems, *Numerical Methods for Partial Differential Equations*, **18** (2002), 374-395.

Department of Mathematics, Wayne State University, Detroit, MI 48202, USA
E-mail: song@math.wayne.edu and gyin@math.wayne.edu and zzhang@math.wayne.edu
URL: http://www.math.wayne.edu/∼song and http://www.math.wayne.edu/∼gyin
URL: and http://www.math.wayne.edu/∼zzhang